C(a) following CO desorption indicate that all carbon from dissociative CH_3OH adsorption on Pd(111) leaves the surface as CO. The lack of H_2O desorption and the absence of residual O(a) (<0.1% of a monolayer) following CO desorption indicate that all oxygen from dissociative CH_3OH adsorption on Pd(111) leaves the surface as CO.

Since the above results for $^{12}CH_3{}^{18}OH$ are in good agreement with the literature regarding the behavior of CH_3OH on clean Pd(111),[5,6] the thermal desorption method was used to study the coadsorption of $^{13}CH_3{}^{16}OH$ and $^{12}CH_3{}^{18}OH$ on the Pd(111) surface. The isotopic CO desorption spectra resulting from methanol adsorption at 110 K are shown in Figure 2a-c. In the case of Figure 2a, 2.6×10^{14} molecules/cm^2 of a 50% "$^{13}CH_3{}^{16}OH$" and 50% "$^{12}CH_3{}^{18}OH$" mixture of isotopically labeled methanol molecules was exposed to the surface. This exposure to methanol corresponds closely to that used in ref 1. Separate experiments involving exposures of 100% "$^{13}CH_3{}^{16}OH$" and 100% "$^{12}CH_3{}^{18}OH$" are shown in Figure 2, b and c, respectively, as a control. The percentage yields for each CO isotope are listed in Table I as obtained from the integrated areas of the corresponding CO desorption peaks in Figure 2. Small yields of $^{13}C^{18}O$ are obtained from 100% "$^{13}CH_3{}^{16}OH$" and 100% "$^{12}CH_3{}^{18}OH$" due to isotopic impurities in these alcohols (Figure 2, b and c). The mixture of 50% "$^{13}CH_3{}^{16}OH$" and 50% "$^{12}CH_3{}^{18}OH$" leads to the evolution of 19.0% $^{12}C^{16}O$ and 1.6% $^{13}C^{18}O$. In fact, if one assumes that there is *no isotopic exchange*, the percentage yield for each CO isotope from a mixture of 50% "$^{13}CH_3{}^{16}OH$" and 50% "$^{12}CH_3{}^{18}OH$" can be easily calculated based on the data from the separate isotopic methanol adsorption experiments shown in Figure 2, b and c. This calculation assuming no isotopic mixing (see Table I, row d) gives 19.4% of $^{12}C^{16}O$ and 1.5% of $^{13}C^{18}O$; this isotopic composition is very close to the experimental results shown in row c of Table I. The ~20% yield of $^{12}C^{16}O$ in the control and the mixed methanol experiments is higher than expected from the analysis of the methanol isotopic abundance and is due primarily to the adsorption of ~0.007 ML of $^{12}C^{16}O$ from background during these experiments. If complete isotopic exchange had occurred, which would be the case for the C-O bond dissociation in the chemisorbed methanol molecules as proposed in ref 1, *the calculated isotopic CO yields would differ significantly from the yields observed experimentally* (*see row e, Table I*). The lack of production of $^{13}C^{18}O$ is a particularly sensitive indicator that C-O bond scission does not occur.

Similar results to those in Figure 2 were also obtained for methanol adsorption temperatures of 87, 160, 210 and 265 K (data not shown). At 110 K, the adsorption temperature used in ref 1, the isotopic methanol coadsorption experiment was performed also with various methanol exposures from 2 to 34×10^{14} molecules/cm^2. No measurable $^{13}C^{18}O$ production (<3%, due entirely to the abundance of $^{13}C^{18}O$ in the adsorbed methanol isotopic species) was detected for all the methanol exposures used. In addition, adsorbing $^{13}CH_3OH$ using a fluence from our beam doser of 2×10^{14} molecules/s on the Pd(111) surface at 580 and 800 K for more than 600 s left no ^{13}C on the surface, as measured by the O_2-adsorption/CO,CO_2-desorption method.

Finally, to eliminate the possibility that the molecular methanol desorption occurs via $CH_3(a) + OH(a)$ recombination, the isotopic methanol content was analyzed in the two molecular desorption states (cf. Figure 1). No evidence of $^{12}CH_3{}^{16}OH$ or $^{13}CH_3{}^{18}OH$ was found in either methanol desorption state.

In conclusion, we observe no C-O bond scission for the thermal decomposition of methanol on the Pd(111) surface as demonstrated by the absence of isotopic exchange in the desorbing CO and methanol products from coadsorbed $^{13}CH_3{}^{16}OH$ and $^{12}CH_3{}^{18}OH$. The accuracy of measurement is such that if ≥1% of the adsorbed CH_3OH was dissociated, it could be detected by the production of $^{13}C^{18}O$ or isotopically mixed methanol species. This conclusion differs significantly from that of ref 1, where, using different Pd(111) surface cleaning methods and different surface measurement techniques, efficient C-O and scission in either adsorbed CH_3OH or CH_3O is proposed on Pd(111). Our results, in distinction to the conclusions of ref 1, also exclude the possibility of the formation of appreciable surface concentrations of $CH_3(a)$ from CH_3OH, since CO formation from $CH_3(a)$ would be accompanied by isotopic mixing in our experiments.

Acknowledgment. The authors gratefully acknowledge the financial support of the Army Research Office (Contract No. DAAL 03-86-K-0005). L.H. acknowledges the support of a National Science Foundation Postdoctoral Fellowship in Chemistry, Grant CHE-8808082 awarded in 1988. We thank Professor Nicholas Winograd for helpful discussions regarding this work.

Autocatalysis and Apparent Bistability in the Formose Reaction

W. Phillip Huskey[‡] and Irving R. Epstein*

Contribution from the Department of Chemistry, Brandeis University, Waltham, Massachusetts 02254. *Received October 17, 1988*

Abstract: The homogeneous formose reaction has been studied under continuous-flow stirred-tank reactor conditions and under batch conditions. Several classes of mechanisms have been examined, and simulations of a model accounting for the observed autocatalysis and isotope effects in the reaction are presented. Hysteresis loops seen under flow conditions are thought to arise from insufficient observation times.

Under basic conditions in the presence of certain divalent cations, aqueous formaldehyde reacts to form a complex mixture of sugars and other compounds in a process called the formose reaction. The reaction has aroused interest as a potential source of carbohydrates,[1-4] as a model for the prebiotic synthesis of sugars,[5-8] and because of its resemblance to carbohydrate metabolism.[9] Our interest in the reaction derives from the autocatalytic nature of the reaction under batch conditions and from

[‡]Present address: Department of Chemistry, Rutgers, The State University, Newark, NJ 07102.

(1) Mizuno, T.; Weiss, A. H. In *Advances in Carbohydrate Chemistry and Biochemistry*; Wolfram, M. L., Tipson, R. S., Eds.; Academic Press: New York, 1974; Vol. 29, pp 173-227.
(2) Matsuura, T.; Shigemasa, Y.; Nagae, O.; Sakazawa, C.; Nakashima, R. *J. Am. Chem. Soc.* **1978**, *100*, 1309-1310.
(3) Matsumoto, T.; Inoue, S. *J. Chem. Soc., Perkin Trans. 1* **1982**, 1975-1979.

0002-7863/89/1511-3157$01.50/0

hints of chemical instability under flow-reactor (CSTR) conditions.[7,10] In addition, the chemistry of the formose reaction represents a departure from the chemistry of other systems, many containing oxyhalogen compounds, which exhibit the special features of nonlinear dynamics.[11,12]

Much of the early mechanistic work on the formose reaction involved studies of metal ion, solvent, and cocatalyst influences on the sigmoidal loss of formaldehyde under batch conditions,[13-18] This work together with modern chromatographic studies of the products over the course of the formose reaction[8,19-21] supports a general mechanism consisting of aldol condensations, Lobry de Bruyn-Alberda van Ekenstein transformations, and Cannizzaro reactions. The autocatalytic nature of the reaction was best accounted for by Breslow[22] using a mechanism (1) consisting of

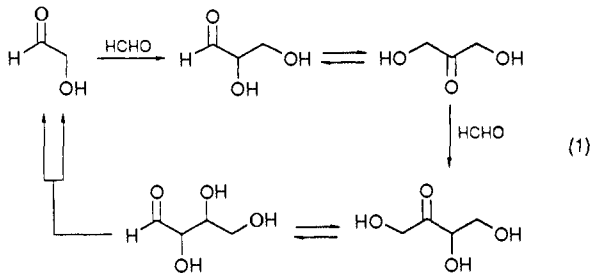

(1)

the formation of an aldotetrose which can degrade to two molecules of glycolaldehyde (the first compound in the cycle) per molecule of tetrose. On the basis of their experimental findings, Harsch et al.[19,23] discount the importance of Breslow's account of autocatalysis. We hoped to learn more about the origins of the autocatalysis and the apparent bistability of the CSTR-formose reaction through CSTR studies in conjunction with computer simulations of mechanistic models.

Weiss and John[10] and Decker[7] have published observations of formose reactions in continuous-flow, stirred-tank reactors (CSTR) that led these authors to conclude that the reaction under flow conditions can produce chemical instabilities[10] and bistability.[7] We set out to explore the CSTR behavior of the formose reaction with the intention of learning subtle details about the mechanism of this complex reaction. Our observations and computer simulations have led us to conclude that hysteresis loops observed in the CSTR-formose reaction do not arise from chemical instabilities, but result from chemical reactions that are slow relative to the time scale of the experiments. In the process of analyzing our observations, we have arrived at new models showing bistability, and we have built a model for the autocatalytic phase of the formose reaction that is consistent with many experimental results.

Experimental Section

Materials. Formaldehyde solutions were prepared by subliming paraformaldehyde (Aldrich) under nitrogen while allowing the gas to pass through a glass tube into a flask of distilled water. Formaldehyde concentrations in reactant solutions were determined by using sulfite titrations as described by Walker.[40] Formaldehyde solutions were prepared no more than 1 day before use. Calcium acetate solutions were prepared based on the apparent molecular weight of individual lots of the salt as obtained from Aldrich. Apparent molecular weights were determined by using EDTA titrations to measure calcium concentrations according to published procedures.[41] Other materials were used as obtained from Aldrich or Fisher.

Reactor Studies. A CSTR can be used to study the dynamical behavior of chemical systems under conditions that are open to the flow of mass. Typically, reactants are continuously pumped into a reactor designed to maintain a constant volume, and as the reaction occurs in the presence of vigorous stirring, a fraction of the mixture of reactants, products, and intermediates is continually flowing out of the reactor. In many chemical systems, the rate of the chemical reaction will eventually balance the rate of material flow into and out of the reactor and a steady state will be maintained until either the feed solutions are exhausted or a change is introduced into the complete reactor system. The steady state can be characterized, for example, by measuring "responses" such as reactant or product concentrations. A typical CSTR study involves the measurement of responses as a function of one or more "constraints" on the reactor such as feed concentration or flow rate. In our work, we have measured steady-state formaldehyde concentration (response) as we varied the residence time (constraint), which is the flow rate divided by reactor volume. Hysteresis-loop experiments were conducted by subjecting the reactor to a series of flow rates forming a complete loop of values from low to high and back to low residence times. At each residence time, the system was allowed to reach what appeared to be a true steady state as judged by invariant concentrations of formaldehyde in the reactor. A more detailed description of our reactor studies is provided below.

A water-jacketed cylindrical glass reactor, fitted with a Teflon top securing platinum and calomel electrodes (Radiometer), two feed-stream tubes, a thermistor probe, and an aspirated overflow tube, was used for CSTR studies of the homogeneous formose reaction. Reactor contents were stirred from below by using a magnetic stirrer (600-700 rpm as measured with a stroboscope). The reactor temperature was maintained at 48 °C with a Haake water heater/circulator and was continually monitored with a thermistor thermometer and a probe placed in the reactor. When changes in flow rates were made, the temperature of the reactor could be maintained to ±0.5 °C by manually adjusting the heater. The volume of the reactor with all components in place was 20.0 mL. Two polypropylene feed tubes to the reactor were connected to a Sage Model 375A peristaltic pump with silicone pump tubing. The potential difference between the platinum and calomel electrodes was monitored on a chart recorder.[42] Changes of nearly 0.2 V could be seen as the system switched from high to low formaldehyde concentration. To determine formaldehyde concentration in the presence of formose products, 1-mL aliquots of the overflow were collected by way of a three-way valve in the overflow aspiration line. The sample was collected in a polyethylene vial placed in an ice bath. Formaldehyde concentrations were determined immediately after collecting a sample by the chromotropic acid method.[43]

Batch Reactions. The loss of formaldehyde under batch conditions was monitored by the discontinuous chromotropic acid method mentioned above. A 5-mL portion of 0.234 M sodium hydroxide at 48 °C was added to 5 mL of 0.6 M formaldehyde in 0.073 M calcium acetate, also at 48 °C. The reaction was conducted in a glass vial placed in a water-jacketed vessel attached to a heater/circulator. Reaction mixtures were continually stirred with a magnetic stirrer. Over the course of the reaction 0.5-mL aliquots of the reaction mixture were removed for analysis.

Dimethoxymethane Reaction. Sodium methoxide (1.2 M) in methanol-*O-d* (Aldrich) was prepared under nitrogen by adding clean sodium to the solvent. A solution of 0.59 M sodium methoxide and 3.78 M dimethoxymethane was prepared from the more concentrated methoxide solution and methanol-*O-d*. A few milliliters of this solution and a 3.72 M dimethoxymethane solution in methanol-*O-d* (with no methoxide present) were sealed under nitrogen in separate NMR tubes.

Numerical Simulations. Simulations were carried out by using local Fortran programs employing the GEAR[44] algorithm.

(4) Castells, J.; Geijo, F.; López-Calahorra, F. *Tetrahedron Lett.* **1980**, *21*, 4517-4520.
(5) Gabel, N. W.; Ponnamperuma, C. *Nature* **1967**, *216*, 453-455.
(6) Reid, C.; Orgel, L. E. *Nature* **1967**, *216*, 455.
(7) Decker, P. *Ann. N.Y. Acad. Sci.* **1979**, *316*, 236-250.
(8) Decker, P.; Schweer, H.; Pohlmann, R. *J. Chromatogr.* **1982**, *244*, 281-291.
(9) Degani, C.; Halmann, M. *Nature* **1967**, *216*, 1207.
(10) Weiss, A. H.; John, T. *J. Catal.* **1974**, *32*, 216-229.
(11) Epstein, I. R.; Kustin, K. *Struct. Bonding* **1984**, *56*, 1-33.
(12) Epstein, I. R.; Orbán, M. In *Oscillations and Traveling Waves in Chemical Systems*; Field, R. J., Burger, M., Eds.; Wiley: New York, 1985; Chapter 8.
(13) Langenbeck, W. *Naturwissenschaften* **1942**, *30*, 31-34.
(14) Pfeil, E.; Schroth, G. *Chem. Ber.* **1952**, *85*, 293-307.
(15) Ruckert, H.; Pfeil, E.; Scharf, G. *Chem. Ber.* **1965**, *98*, 2558-2565.
(16) Weiss, A. H.; Seleznev, V. A.; Sakharov, M. M.; Krylov, O. V.; Gorokhovatsky, Y. B.; Evmenenko, N. P. *J. Catal.* **1977**, *48*, 354-364.
(17) Shigemasa, Y.; Shimao, M.; Sakazawa, C.; Matsuura, T. *Bull. Chem. Soc. Jpn.* **1977**, *50*, 2138-2142.
(18) Shigemasa, Y.; Fujitani, T.; Sakazawa, C.; Matsuura, T. *Bull. Chem. Soc. Jpn.* **1977**, *50*, 1527-1531.
(19) Harsch, G.; Voelter, W.; Bauer, H. *Z. Naturforsch., B* **1977**, *32b*, 826-832.
(20) Harsch, G.; Harsch, M.; Bauer, H.; Voelter, W. *Z. Naturforsch., B* **1983**, *38b*, 1269-1280.
(21) Harsch, G.; Bauer, H.; Voelter, W. *Liebigs Ann. Chem.* **1984**, 623-635.
(22) Breslow, R. *Tetrahedron Lett.* **1959**, 22-26.
(23) Harsch, G.; Harsch, M.; Bauer, H.; Voelter, W. *Z. Naturforsh., B* **1983**, *38b*, 1269-1280.

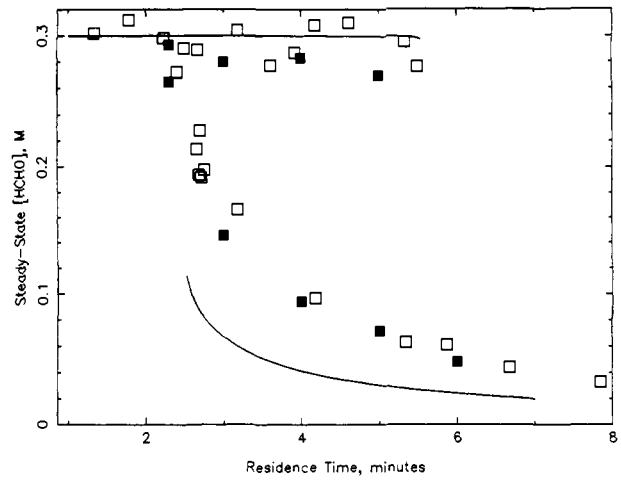

Figure 1. Hysteresis loops seen in the CSTR-formose reaction at 48 °C. Two feed streams were fed into the reactor at approximately the same flow rate using a peristaltic pump. One feed stream contained 0.6 M formaldehyde and 0.073 M calcium acetate. The other feed stream contained 0.233 M sodium hydroxide. The open squares represent a collection of numerous experiments for which apparent steady states were monitored between 30 min to several hours. The solid squares depict a hysteresis loop obtained at a single sitting during which each steady state was observed for a 2-h period before moving to the next residence time. For the solid squares, the hysteresis experiment begins at short residence times. The solid line is the best simulation of the data using model D of Table I ($k_1 = 1 \times 10^{-5}$ M^{-1} min^{-1}, $k_2 = 20$ M^{-1} min^{-1}, $k_3 = 5.6$ min^{-1}, $k_4 = 0.02$ min^{-1}).

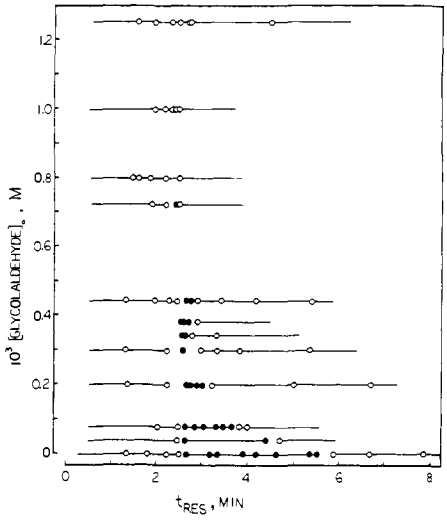

Figure 2. Narrowing of the region of apparent bistability (filled circles) with increasing feed glycolaldehyde concentration. Reactor conditions are the same as those of Figure 1, except the formaldehyde-containing feed stream contained twice the glycolaldehyde concentration plotted in the diagram.

Results

Apparent steady states observed in the CSTR as a function of the reactor residence time are presented in Figure 1. Formaldehyde concentrations were determined after the potential at a platinum electrode appeared to be constant, generally after 30–120 min. The data obtained in this way define a hysteresis loop that grows narrower as the feed concentration of glycolaldehyde is increased (Figure 2). The many data points in Figure 1 were not collected in a single experiment; instead, the figure represents an accumulation of five separate hysteresis-loop experiments. The path outlined by the solid squares depicts a hysteresis loop obtained in a single experiment beginning at low residence times, stepping up to higher residence times, and finally returning in steps to the original residence time. On this loop, steady states were observed for 2 h before proceeding to the next residence time in the series. The origin of these hysteresis loops could well lie in genuine bistability of the formose reaction at low cocatalyst (glycolaldehyde) concentrations.

Table I. Selected Crude Mechanisms Examined as Potential Models for Bistability in the Formose Reaction[a]

model	mechanism[b]	f	g	instability possible
A	$2x_1 \rightarrow x_2$	0	1	yes
	$fx_1 + x_2 \rightarrow 2x_2$	0.5	1	yes
	$2x_2 \rightarrow p_1$	1	1	no
	$gx_1 + x_2 \rightarrow p_2$	2	1	no
		1	2	yes
B	$2x_1 \rightarrow x_2$			no
	$x_1 + x_2 \rightarrow x_3$			
	$x_1 + x_3 \rightarrow x_4$			
	$x_4 \rightarrow 2x_2$			
C	$2x_1 \rightarrow x_2$			yes
	$x_1 + x_2 \rightarrow x_3$			
	$x_3 \rightarrow 2x_2$			
	$x_1 + x_3 \rightarrow x_4$			
	$x_4 \rightarrow 2x_3$			
D	$2x_1 \rightarrow x_2$ (k_1)			yes
	$x_1 + x_2 \rightarrow x_3$ (k_2)			
	$x_1 + x_3 \rightarrow x_4$ (k_2)			
	$x_1 + x_4 \rightarrow x_5$ (k_2)			
	$x_1 + x_5 \rightarrow x_6$ (k_2)			
	$x_4 \rightarrow 2x_2$ (k_3)			
	$x_6 \rightarrow 2x_3$ (k_4)			

[a] All models are CSTR models (all reactants, intermediates, and products flow out of the reactor with the same rate constant) with x_1 as the only feed species. [b] Species labeled with p represent inert products.

We examined numerous skeletal representations of the formose reaction in an effort to determine the kinds of feedback capable of yielding bistable mechanisms. Some of these models are presented in Table I. We used a combination of Fortran programs and MACSYMA[24] routines based on methods developed by Clarke[25] to eliminate mechanisms that could not exhibit bistability. Breslow's mechanism (with CSTR flow reactions included, model B), for example, does not contain the feedback necessary to give bistability. However, extension of Breslow's model to include the formation and breakdown of six-carbon sugars is sufficient to produce bistability.

The solid lines in Figures 1 and 2 show our best efforts to simulate the formose reaction under batch and CSTR conditions. Modifications to the model, which included the separate rate constants for each of the chain-forming steps, the addition of Cannizzaro and dehydration reactions, and the addition of all possible feedback decompositions for the four-, five-, and six-carbon products could not produce a better fit to the experimental observations. Models that incorporated up to ten-carbon sugars also failed to improve the simulations as did models that included the formation of branched-chain compounds.

If the skeletal mechanisms like those of Table I are compared with more detailed descriptions of the chemistry occurring in the formose reaction, it is apparent that the skeletal models include an implicit assumption that the rate-limiting step in the sugar-forming aldol reactions is the addition of formaldehyde to enols, rather than the proton-transfer reaction leading to the enol. We tested this assumption by monitoring the formose reaction under batch conditions using deuterated formaldehyde and deuterium oxide. The results, shown in Figure 3, suggest that there are large normal substrate isotope effects, and large inverse solvent isotope effects on the rate-limiting processes in the autocatalytic phase of the reaction. Both results are consistent with rate-limiting proton transfer to solvated hydroxide ion.[26,27] Furthermore, the

(24) MACSYMA is a large symbolic manipulation program developed at the M.I.T. Laboratory for Computer Science. Development of the program was supported from 1975 to 1983 by the National Aeronautics and Space Administration under Grant NSG 1323, by the Office of Naval Research under Grant N00014-77-C-0641, by the U.S. Department of Energy under Grant ET-78-C-02-4687, and by the U.S. Air Force under Grant F49620-79-C-020; since 1982 the program has been supported by Symbolics, Inc., of Cambridge, MA. MACSYMA is a trademark of Symbolics, Inc.

(25) Clarke, B. L. *Adv. Chem. Phys.* **1980**, *43*, 1–215.

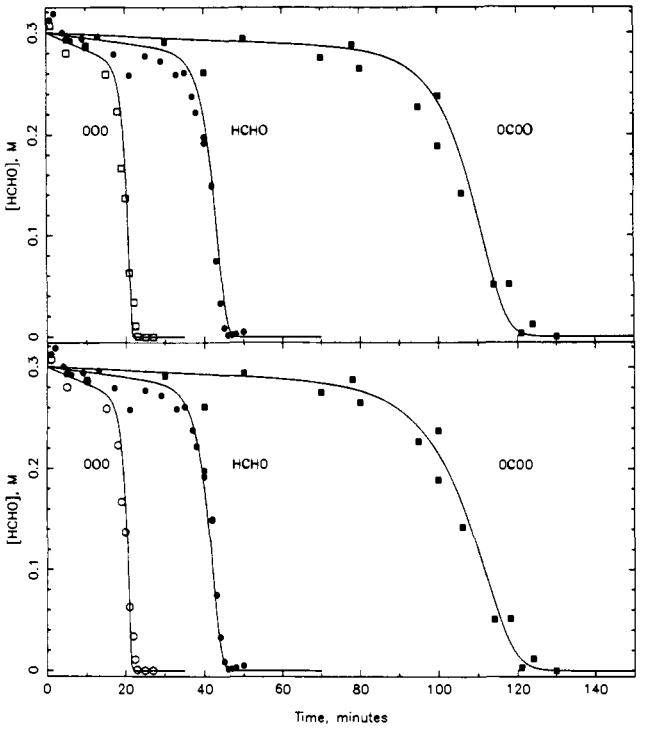

Figure 3. Batch formose reactions at 48 °C using initial concentrations of 0.3 M formaldehyde, 0.036 M calcium acetate, and 0.151 M sodium hydroxide. The upper panel shows the fit of model F with no initial glycolaldehyde (x_2) present (HCHO: $k_1 = 7.5$, $k_2 = 2.5$, $k_3 = 3 \times 10^6$, $k_4 = 1000$, $k_5 = 0.003$, $k_6 = 1 \times 10^{-8}$, $k_7 = 2 \times 10^8$, $k_8 = 2 \times 10^7$. DCDO: $k_1 = 2.8$, $k_2 = 0.9$, $k_3 = 3 \times 10^6$, $k_4 = 1000$, $k_5 = 0.001$, $k_6 = 1 \times 10^{-8}$, $k_7 = 2 \times 10^8$, $k_8 = 2 \times 10^7$. DOD: $k_1 = 12$, $k_2 = 4$, $k_3 = 5 \times 10^5$, $k_4 = 1000$, $k_5 = 0.01$, $k_6 = 1 \times 10^{-8}$, $k_7 = 2 \times 10^8$, $k_8 = 2 \times 10^7$). The lower panel shows the best simulations of model E with a small amount of glycolaldehyde present and $k_6 = 0$ (HCHO: initial $x_2 = 4 \times 10^{-9}$ M, with $k_6 = 0$ remaining k's are the same as HCHO for top panel. DCDO: initial $x_2 = 2 \times 10^{-7}$ M, $k_1 = 2.1$, $k_2 = 0.7$, and remaining k's the same as above. DOD: initial $x_2 = 4 \times 10^{-9}$ M, k's are the same as above). The units for all first-order rate constants listed above are min^{-1}, and the units for the second-order rate constants are M^{-1} min^{-1}.

lack of deuterium incorporation into formose products when the reaction is conducted in deuterium oxide[28] supports a mechanism whereby proton transfer limits the rate.

The extended Breslow mechanism was modified to include explicit proton-transfer and formaldehyde-addition steps in the sequence of building carbon chains. Sets of rate constants were found that produced bistability and maintained rate-limiting proton transfer for most of the reaction, but there was no improvement in the agreement with the experimental observations. The fit to the lower branch in Figure 1 was always poor.

We next conducted very long experiments in an effort to test whether or not our observations in the flow reactor reflected true steady states. The results of Figure 4 show the time for a change in formaldehyde concentration to half the initial feed value. The reactor was filled and then the pump was adjusted to give the residence times shown for each point in the figure. The curves for these transitions from the high formaldehyde state to the low formaldehyde state are characterized by long induction periods, followed by more rapid consumption of formaldehyde until the low state is reached. The solid squares in Figure 4 show points collected when the two reactant feed streams were merged with a T-tube just prior to entry of reactor. Such "premixing" has been found to have a significant effect on the dynamics of some reactants in a CSTR.[29,30] The states along the upper branch of

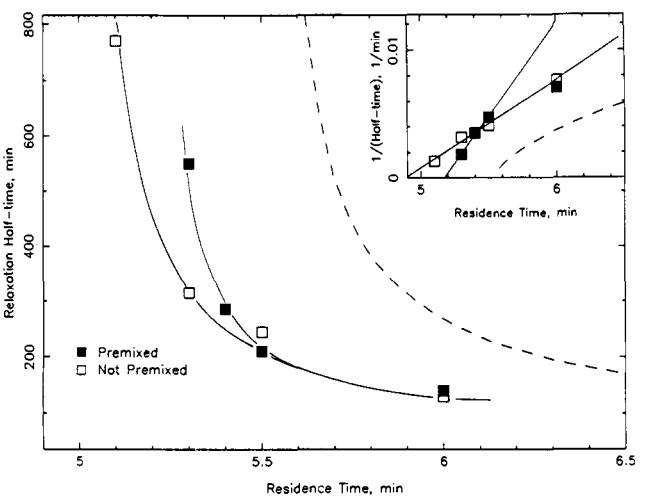

Figure 4. Half-time for a transition from high formaldehyde to low formaldehyde for the reactor conditions described in Figure 1. The dashed line shows the behavior expected for model D using the parameters of Figure 1.

Figure 1 appear to be stable or they relax in more time than can be reasonably expended to monitor and feed a reactor in the laboratory.

On the lower branch, the states at residence times of 2.4 and 2.7 min were monitored for extra long times. The reactor was first operated with a residence time of 6.0 min, and 2.0 mL of a formose product mixture was injected into the reactor. The formaldehyde concentration switched from 0.3 M to 0.042 M, and after 2 h, the pump was changed to give a residence time of 2.4 or 2.7 min. For the change to 2.4 min, the formaldehyde concentration increased in an exponential fashion to 0.272 M with a half-time of about 10 min. The final concentration remained unchanged for 7.8 h. For the change to 2.7 min, a final formaldehyde concentration of 0.252 M was reached with a half-time of <20 min and remained constant over an observation time of 5.3 h.

Discussion

Origin of Autocatalysis. A viable mechanism for the formose reaction must reproduce the sigmoidal batch progress curves indicative of autocatalysis. Breslow's mechanism[22] (eq 1) provides a reasonable basis for the sigmoidal progress curves, and we sought to extend his idea to give a more complete description of the autocatalytic phase of the reaction.

It appears that feedback reactions similar to the tetrose-cleavage reaction (1) proposed by Breslow[22] are needed to explain the autocatalysis. We set out to build and simulate a model for the autocatalytic phase of the formose reaction that would explain the batch reactions and the isotope effects and that would truncate naturally with sugar molecules of no more than seven or eight carbon atoms. Our previous models were artificially terminated with low molecular weight sugars for simplicity and because high molecular weight sugars, while they may be formed in the reaction, have not been identified. We built a model that met our specifications by assuming that (1) enol or enolate species could be treated as steady-state intermediates, (2) trapping of enols by formaldehyde is faster than trapping by water to regenerate aldehydes and ketones, (3) trapping of enols by other intermediates and products of the reaction can be ignored during the autocatalytic phase, (4) retro-aldol reactions only occur when formaldehyde is not one of the products, and (5) the retro-aldol cleavage step is slower than enol trapping by formaldehyde but faster than enol-generating proton transfer. The resulting model is shown in Figure 5. The aldotetrose proposed by Breslow[22] to be the source of autocatalysis does not form in our mechanism, but the

(26) Melander, L.; Saunders, W. H., Jr. *Reaction Rates of Isotopic Molecules*; Wiley: New York, 1980.
(27) Schowen, R. L. *Prog. Phys. Org. Chem.* **1972**, *9*, 275–332.
(28) Zhemecki, S. B.; LaPierre, R. B.; Weiss, A. H.; Sakharov, M. M. *J. Catal.* **1977**, *50*, 455–463.
(29) Menzinger, M.; Boukalouch, M.; De Kepper, P.; Boissonade, J.; Roux, J. C.; Saadaoui, H. *J. Phys. Chem.* **1986**, *90*, 313–315.
(30) Luo, Y.; Epstein, I. R. *J. Chem. Phys.* **1986**, *85*, 5733–5740.

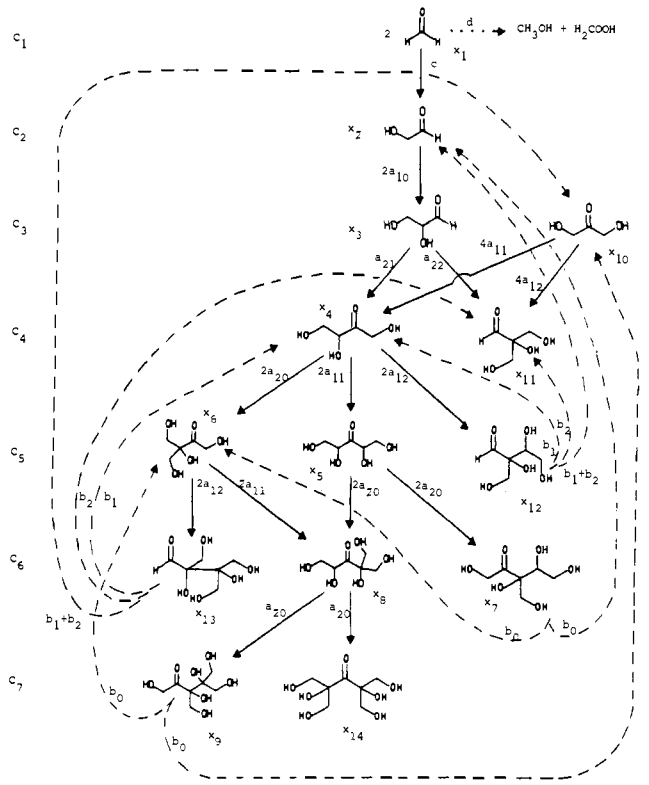

Figure 5. Formose reaction model E. The solid arrows show aldol condensations with formaldehyde, the dashed lines show retro-aldol reactions, and the dotted line is a Cannizzaro reaction. See the text for more details.

general concept of his model is represented in the retro-aldol reactions of three other compounds.

Our assumptions can be justified to some extent by existing mechanistic work on related reactions. We have assumed that enols or enolate ions are steady-state intermediates in order to minimize the number of species that must be treated explicitly in the model. Enols are known to be reactive species, although many can be trapped and studied,[31] and it is reasonable to expect that these compounds do not accumulate during the autocatalytic phase of the formose reaction. Our choices for rate constants used for the breakdown and formation of the enol intermediates in the simulations (Figure 3) ensure that these species will not accumulate.

Because we have assumed that trapping of enol species by formaldehyde is faster than trapping by water, Lobry de Bruyn–Alberda van Ekenstein transformations are not present in our model. After the autocatalytic phase, when formaldehyde concentrations are low, these isomerization reactions would be expected to be more prevalent. This assumption is consistent with our observations of the effect of substitution of deuterium for hydrogen on formaldehyde and with the low level of deuterium found in formose products when the reaction is conducted in deuterium oxide.[28] Omission of enol trapping by formose products simplifies our model, and it is justified by the low concentrations of any given product with respect to the formaldehyde concentration, especially during the first half of the autocatalytic phase. Rapid trapping of enols by formaldehyde also rationalizes the absence of formaldehyde-forming retro-aldol reactions. Since the resulting enol would only be trapped again by formaldehyde, it is hard to imagine that the incorporation of reversible reactions of formaldehyde with enols would add anything new to the dynamics of the reaction.

Our final assumptions, that the retro-aldol cleavage step is slower than enol trapping by formaldehyde but faster than enol-generating proton transfer, serve to simplify the model. With enol trapping faster than the carbon–carbon bond-breaking step, the rate constant for the formation of products from the enols generated in the retro-aldol reactions will simply be the rate constant for the actual retro-aldol step. Otherwise, it is necessary to introduce another parameter in the model to account for aldol reactions that were excluded with the third assumption. Lastly, the model terminates with seven-carbon carbohydrates if retro-aldol reactions are faster than enol-forming proton transfers. Without this assumption, our formula for the generation of a mechanism will yield a model consisting of carbon chains growing continually longer without a rational termination point.

Table II. Parameters for Formose Model E

parameter in Figure 5	relationship to rate constants[a]
a_{10}[b]	$k_1k_7x_1/(2k_3 + x_1(k_7 + k_7))$
a_{20}	$k_2k_8x_1/(2k_3 + x_1(k_8 + k_8))$
a_{11}	$k_1k_7x_1/(2k_3 + x_1(k_7 + k_8))$
a_{12}	$k_1k_8x_1/(2k_3 + x_1(k_7 + k_8))$
a_{21}	$k_2k_7x_1/(2k_3 + x_1(k_7 + k_8))$
a_{22}	$k_2k_8x_1/(2k_3 + x_1(k_7 + k_8))$
b_0	k_4
b_1	$k_4k_7/(k_7 + k_8)$
b_2	$k_4k_8/(k_7 + k_8)$
c	k_6
d	k_5

[a] k_1 and k_2 are rates for enol-forming proton transfers from primary and secondary carbons, k_3 is for the proton transfer in the reverse direction, k_4 is for the retro-aldol reaction, k_5 is for the Cannizzaro reaction, k_6 is for dimerization of formaldehyde, and k_7 and k_8 are for formaldehyde trapping of enols to form new secondary and tertiary carbon centers. [b] The factor of 2 appears with k_3 because the proton-transfer reaction leading to isomers of a carbonyl compound was included in the steady-state expressions for enols, although the isomers were excluded from the model.

Application of our assumptions leads to model E shown in Figure 5. Rate constants for model E giving satisfactory fits to batch reactions are provided in the legend of Figure 3. The relationships between rate constants and the parameters of Figure 5 are given in Table II. The coefficients attached to the parameters account for the differences in the number of identical reaction sites among reactants and intermediates. The solid lines of the figure trace the path of formaldehyde polymerization through successive aldol condensations, the dashed lines show retro-aldol reactions, and the dotted line marks the only Cannizzaro reaction in model E. The rate equations for model E can be derived by applying the rules of mass-action kinetics (remembering that formaldehyde is consumed in each aldol reaction, and in the trapping of enols produced in the retro-aldol reactions), using the parameters of Figure 5 as rate constants. The exceptions to this formula are the rate terms for the loss of the species undergoing retro-aldol cleavage. These species are consumed with only the rate constants b_0 or the sum $b_1 + b_2$.

Crude comparisons for some of the values for rate constants shown in the legend of Figure 3 can be made with literature values. The rate constants for enol-producing proton-transfer reactions (k_1 and k_2) can be compared, for example, with k_{OH} for enolization of acetone,[32] 0.22 M^{-1} s^{-1} at 25 °C. At our concentration of hydroxide ion, and with different time units, a value of 1.6 min^{-1} can be compared to our values of 7.5 and 2.5 min^{-1}. The comparison is fair considering the differences in temperature and uncertainties about the influence of calcium salts present in the formose reaction. Note that our k_1 and k_2 differ by a factor of 3. It was necesary to introduce differences in the rate constants for proton transfer from primary and secondary carbon atoms in order to see sigmoidal progress curves. The factor of 3 was chosen based on the differences in rate constants for the iodination of dihydroxyacetone and glyceraldehyde catalyzed by acetate.[33] It was also necessary to introduce different rate constants for addition

(31) Capon, B.; Guo, B. Z.; Kwok, F. C.; Siddhanta, A. K.; Zucco, C. *Acc. Chem. Res.* **1988**, *21*, 135–140.

(32) Chiang, Y.; Kresge, A. J.; Tang, Y. S. *J. Am. Chem. Soc.* **1984**, *106*, 460–462.

(33) Lien, L.; Huskey, W. P., unpublished observations.

of formaldehyde to enol species depending on whether a new secondary (k_7) or tertiary (k_8) carbon center was produced. The rate constant for proton transfer to the enol of acetone has also been measured,[33] 3×10^6 min^{-1} at 25 °C, and we chose to use this value without change.

Our rate constant for the Cannizzaro reaction ($k_6 = 0.003$ min^{-1}) compares well with a value of 0.005 min^{-1} computed with the rate law of Martin[34] for the reaction of formaldehyde at 40 °C. The rate constant used for the retro-aldol reaction ($k_4 = 1000$ min^{-1}) is considerably greater than a value estimated from the cleavage of 3-methyl-3-hydroxybutanal,[35] 1.2 min^{-1} at 25 °C. We arbitrarily set k_4 to be 1000 to maintain the condition of our last assumption (that enol-forming proton transfer be slower than retro-aldol cleavages), which was introduced to build a model that terminates naturally. Lower values of k_4 still yield sigmoidal curves on our model, but our termination of the scheme with the species x_7 and x_9 becomes artificial. Given the differences in temperature, substrate structure, and the presence of calcium salts in the formose reaction, it is not unreasonable to expect that k_4 could be substantially larger than 1.2 min^{-1}.

The rate constants of the simulations in Figure 3 correspond to reasonable isotope effects on the individual chemical steps. The substrate isotope effect (k_H/k_D) on the enol-forming proton transfer is 2.7, a value in agreement with expectations for primary hydrogen isotope effects.[26] The only other nonunit substrate isotope effect is a value of 3 for the Cannizzaro reaction, and it compares well with a value of 1.8 reported for the Cannizzaro reaction with benzaldehyde.[36] The solvent isotope effects (k_{HOH}/k_{DOD}) are also in agreement with conventional expectations. The isotope effects on the enol-forming proton-transfer reactions and the Cannizzaro reaction are inverse (0.6 and 0.3), as would be expected if desolvation of hydroxide ions occurs in these reactions.[27] A solvent isotope effect of 0.53 has been reported for the Cannizzaro reaction with benzaldehyde, for example.[37] Finally, the rate constants of Figure 3 give a normal solvent isotope effect of 6 for the proton transfer from water to enol, in agreement with expectations for a primary effect.

Model E of Figure 5 can also be used to make a few predictions concerning formose products. On the model, species x_{11} and x_{14} would be expected to accumulate, at least during the autocatalytic phase of the reaction. Species x_{11}, 2,3-dihydroxy-2-(hydroxymethyl)propanal, has been identified as a formose product.[8,38] Species x_{14} is a heptose, and unidentified heptoses have been found in formose product mixtures.[8]

The initial reaction of model E, the dimerization of formaldehyde to form glycolaldehyde, would be expected to be extraordinarily slow (our choice of a rate constant corresponds to a half-life of >300 years). The initial reaction could involve a proton transfer from the hydrate of formaldehyde to hydroxide ion followed by addition of the formaldehyde -hydrate carbanion to formaldehyde. We used dimethoxymethane (3.78 M) in the presence of sodium methoxide (0.59 M) in methanol-*O*-*d* as a model for a proton transfer from formaldehyde hydrate. After 152 days, we could see no evidence for exchange of the methylene protons of dimethoxymethane with the deuterium of the solvent. Using a detection limit of a 5% change, we can state that the rate constant for this proton-transfer reaction involving methoxide is $<3.8 \times 10^{-8}$ M^{-1} min^{-1}. While our NMR experiment is inconclusive concerning the role of a slow proton transfer in the initial step of the formose reaction, Socha et al.[39] have proposed that

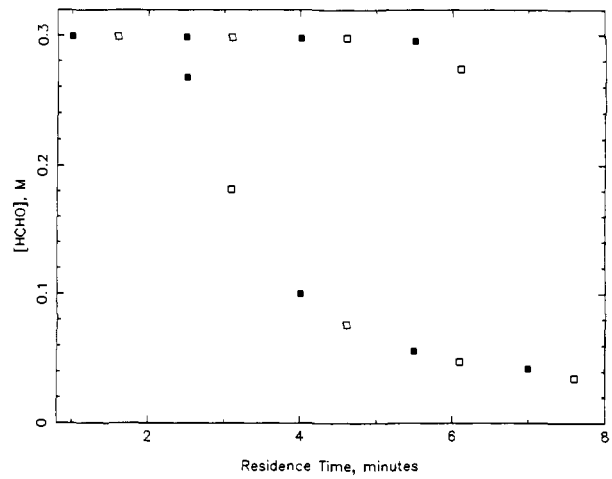

Figure 6. Simulation of an artificial hysteresis loop using model E with the HCHO parameters listed in Figure 3 for the case with no initial glycolaldehyde. When 4×10^{-9} M glycolaldehyde is used with $k_6 = 0$, the results are nearly superimposable. The open and filled squares represent two separate simulated experiments with 30-min waits between changes in residence times.

the formose reaction is initiated by carbohydrate impurities in the reactants. Our simulations do not change significantly if we set k_6 to zero and set the initial concentration of any species (other than x_{11} or x_{14}) in Figure 5 to values on the order of 10^{-9} M. The bottom panel of Figure 3 shows the simulations with $k_6 = 0$ and low initial concentrations of glycolaldehyde (x_2).

It is important to remember that model E represents a simplified account of only the autocatalytic phase of the formose reaction. To the extent that the assumptions of the model hold true, the dynamics of the formose reaction can be explained with a model containing only 14 species and 8 rate constants. If the assumptions do not hold up, autocatalytic models merely become more complex, with more species and more reactions added to the basic core of model E.

Apparent Bistability. Our CSTR studies of the formose reaction do not allow us to reach firm conclusions concerning the presence of chemical bistability in this reaction under flow conditions. We favor the interpretation that the hysteresis loop results from insufficient observation times along the high-formaldehyde branch of the experiment, based on our inability to match the shape of the curve with bistable models reflecting the chemistry of the formose reaction. This is not a strong argument, but it is very simple to generate loops with the shape of the data in Figure 1 by reducing the simulation times at each point for an autocatalytic model. Figure 6 shows the results of a simulation with shortened observation times using model E (with CSTR flow terms added).

Model E is unable to match the experimental half-times for the transition from high to low formaldehyde (Figure 4) under reactor conditions, however. The observation times necessary to produce the loop in Figure 6 are 30 min per point. At 60 min per point, for example, the simulated points all lie along the lower branch of the figure. Mixing effects[29] might account for the discrepancies, although our experiments with reactants mixed just prior to the reactor entry (solid squares in Figure 4) give results that are barely distinguishable from the other results.

We conclude that the hysteresis loops observed with the CSTR-formose reaction, because their shapes resemble simulations with insufficient observation times, do not result from chemical bistability. The observation times necessary to eliminate the

(34) Martin, R. J. L. *Aust. J. Chem.* **1954**, *7*, 335–347.
(35) Guthrie, J. P.; Dawson, B. A. *Can. J. Chem.* **1983**, *61*, 171–179.
(36) Wiberg, K. B. *J. Am. Chem. Soc.* **1954**, *76*, 5371–5375.
(37) Swain, C. G.; Powell, A. L.; Lynch, T. J.; Alpha, S. R.; Dunlap, R. P. *J. Am. Chem. Soc.* **1979**, *101*, 3584–3587.
(38) Castells, J.; Calahorra, F. L.; Domingo, L. *Tetrahedron Lett.* **1985**, *26*, 5457–5458.
(39) Socha, R. F.; Weiss, A. H.; Sakharov, M. M. *React. Kinet. Catal. Lett.* **1980**, *14*, 119–128.
(40) Walker, J. F. *Formaldehye* (American Chemical Society Monograph Series); Reinhold, New York, 1964; pp 486–487.
(41) Kodama, K. *Methods of Quantitative Inorganic Analysis*; Wiley-Interscience: New York, 1963; p 389.
(42) Shigemasa, Y.; Shimao, M.; Sakazawa, C.; Matsura, T. *Bull. Chem. Soc. Jpn.* **1975**, *48*, 2099-2102.
(43) Altshuller, A. P.; Miller, D. L.; Sleva, S. F. *Anal. Chem.* **1962**, *34*, 621–625.
(44) Gear, C. W. *Numerical Initial Value Problems in Ordinary Differential Equations*; Prentice-Hall: Englewood Cliffs, NJ, 1971; Chapter 11. Hindmarsh, A. C. Gear: Ordinary Differential Equation Solver, Technical Report No. UCM-30001, Rev. 2, Lawrence Livermore Laboratory, 1972.

observation of hysteresis are so long, however, that on a time scale of many days, the system is effectively bistable.

Acknowledgment. This work was supported by the National Science Foundation (Grants CHE 8419949 and CHE 8800169) and by a National Institutes of Health Postdoctoral Fellowship (Grant GM 10543) to W.P.H. We thank Robert Olsen, Johannes Reiter, John Rinzel, and Toby Sommer for helpful discussions.

Registry No. D, 7782-39-0.

A Transient Infrared Spectroscopy Study of Coordinatively Unsaturated Ruthenium Carbonyls

Paula L. Bogdan and Eric Weitz*

Contribution from the Department of Chemistry, Northwestern University, Evanston, Illinois 60208. *Received October 24, 1988*

Abstract: Transient infrared spectroscopy is used to study coordinatively unsaturated $Ru(CO)_x$ products formed by excimer laser photolysis of gas-phase $Ru(CO)_5$. Both $Ru(CO)_4$ and $Ru(CO)_3$ are photoproducts of 248- and 351-nm irradiation of $Ru(CO)_5$. This is the first report of direct observation of unsaturated $Ru(CO)_x$ species. Unlike the well-known $Fe(CO)_4$ fragment, the high reactivity of the $Ru(CO)_x$ species has precluded their observation in cryogenic studies. The rate constants for reaction of $Ru(CO)_4$ and $Ru(CO)_3$ with CO are $(2.8 \pm 0.8) \times 10^{-11}$ and $(7.6 \pm 0.3) \times 10^{-11}$ cm^3 molec^{-1} s^{-1}, respectively. These rate constants are $\sim 10^3$ greater than that for the reaction of $Fe(CO)_4$ with CO and can be rationalized in terms of the spin states of the reactants and products. Formation of a dinuclear complex, $Ru_2(CO)_9$, is also observed. Comparison of the distribution of $M(CO)_x$ fragments at different UV photolysis wavelengths has implications for the relative bond dissociation energies for carbonyl ligands on a ruthenium versus an iron center.

I. Introduction

Metal carbonyls are an important class of inorganic compounds. They can be used to thermally and/or photolytically produce reactive species that can induce homogeneous stoichiometric and catalytic transformations of organic substrates. They are also used as precursors to supported metal aggregates, thin films, and other solid-state materials. The dominant photochemical process for metal carbonyls is ligand dissociation, which provides open, highly reactive, coordination sites at the metal center. Details of the nature of these unsaturated species were first probed with matrix isolation techniques.[1] More recently, transient infrared spectroscopic studies of gas-phase unsaturated metal carbonyl photofragments have provided detailed information about the structure and reaction kinetics of these highly reactive species.[2]

One of the most well-studied of the metal carbonyls is $Fe(CO)_5$; its photofragments exhibit unique properties compared to those of other metal carbonyl compounds.[3,4] While $Fe(CO)_5$ has a singlet ground state, the unsaturated species $Fe(CO)_2$, $Fe(CO)_3$, and $Fe(CO)_4$ have been characterized as possessing triplet electronic ground states.[5] As a result, recombination of $Fe(CO)_4$ and CO to regenerate the singlet parent $Fe(CO)_5$ is comparatively slow. The gas-phase lifetime of $Fe(CO)_4$ in the presence of 100 Torr of CO is a relatively long 0.1 ms. This is in sharp contrast to the group 5 and 6 carbonyls, $V(CO)_6$, $Cr(CO)_6$, and $W(CO)_6$, whose ligand addition reactions take place on a potential energy surface of the same spin multiplicity. In these systems, photofragments have lifetimes on the order of microseconds with only 1 Torr of CO present.[6-8]

Another difference between $Fe(CO)_5$ and the group 6 carbonyls is that, upon 351-nm photolysis, $Fe(CO)_5$ loses two CO ligands while $Cr(CO)_6$ and $W(CO)_6$ give primarily $M(CO)_5$ photofragments. As a result of other studies it has been suggested that the $Fe(CO)_3$–CO bond is anomalously weak.[9] These results are compatible with this suggestion.

Since the electronic properties and product distribution of $Fe(CO)_5$ photofragments are unusual, it is of interest to speculate whether these are peculiar to iron itself or whether they prevail in the group 8 triad. The $M(CO)_5$ homologous series is known; however, the chemistry of $Ru(CO)_5$ and $Os(CO)_5$ has received far less attention than that of $Fe(CO)_5$. A major factor is the instability of the pentacarbonyls of osmium and ruthenium with respect to formation of the well-known $M_3(CO)_{12}$ species. In general, the stability of metal cluster species increases as one descends group 8 owing to an increase in M–M bond strength. Calculations have suggested that, unlike $Fe(CO)_4$, the $Ru(CO)_4$ fragment has a singlet electronic ground state.[10] We have chosen to study the gas-phase photochemistry of $Ru(CO)_5$, to compare and contrast the nature and reactivity of its photofragments with those of $Fe(CO)_5$.

Time-resolved infrared spectroscopy is used to determine the identities of unsaturated fragments following XeF and KrF excimer laser photolysis of $Ru(CO)_5$ and to determine microscopic rate constants for the reaction of these species with CO. Reactions of coordinatively unsaturated ruthenium species with $Ru(CO)_5$ have been observed and are discussed. Based on product distributions as a function of photolysis wavelength, comparisons of relative M–CO bond dissociation energies for iron and ruthenium can be made.

II. Experimental Section

The apparatus used in this study has been previously described.[11-14] Since it is both expensive and inconvenient to prepare and handle the amount of $Ru(CO)_5$ that would be needed for a flow cell, a change in

(1) Hitam, R. B.; Mahmoud, K. A.; Rest, A. J. *Coord. Chem. Rev.* **1984**, *55*, 1.
(2) Weitz, E. *J. Phys. Chem.* **1987**, *91*, 3945.
(3) Poliakoff, M.; Weitz, E. *Acc. Chem. Res.* **1987**, *20*, 408.
(4) Seder, T. A.; Ouderkirk, A. J.; Weitz, E. *J. Chem. Phys.* **1986**, *85*, 1977.
(5) Barton, T. J.; Grinter, R.; Thomson, A. J.; Davies, B.; Poliakoff, M. *J. Chem. Soc., Chem. Commun.* **1977**, 841.
(6) Ishikawa, Y.; Hackett, P. A.; Rayner, D. M. *J. Am. Chem. Soc.* **1987**, *109*, 6644.
(7) Seder, T. A.; Church, S. P.; Weitz, E. *J. Am. Chem. Soc.* **1986**, *108*, 4721.
(8) Ishikawa, Y.; Hackett, P. A.; Rayner, D. M. *Chem. Phys. Lett.* **1988**, *145*, 429.
(9) Engelking, P. C.; Lineberger, W. C. *J. Am. Chem. Soc.* **1979**, *101*, 5570.
(10) Ziegler, T. *Inorg. Chem.* **1986**, *25*, 2721.
(11) Ouderkirk, A. J.; Weitz, E. *J. Chem. Phys.* **1983**, *79*, 1089.
(12) Ouderkirk, A. J.; Wermer, P.; Schultz, N. L.; Weitz, E. *J. Am. Chem. Soc.* **1983**, *105*, 3354.
(13) Ouderkirk, A. J.; Seder, T. A.; Weitz, E. *SPIE Symp. Appl. Lasers Ind. Chem.* **1984**, *458*, 148.
(14) Seder, T. A.; Church, S. P.; Weitz, E. *J. Am. Chem. Soc.* **1985**, *107*, 1432.

0002-7863/89/1511-3163$01.50/0